J. Materials, Conc. Struct., Pavements No. 472/V-20, pp. 119~130, August 1993

MODELING OF CONCRETE DISCONTINUITIES WITH DILATANCY AND SURFACE DEGRADATION

Zhishen WU*, Ahmed M. FARAHAT**
and Tada-aki TANABE***

A new physically motivated constitutive model for the behavior of concrete discontinuities is presented. In the present model, in order to consider a detailed contact mechanism which can clearly express the microscopic features of the concrete discontinuities, the behavior at the contacts between mortar and mortar as well as between aggregate and mortar is distinguished and investigated individually. To simulate all sorts of nonlinearities, two independent hyperbolic surfaces which have Mohr-Coulomb surface as an asymptotic surface for both the plastic potential and the yield function are defined in stress space. The basic material parameters;cohesion, internal friction angle, dilatancy angle and tensile strength are varied according to the accumulated damage. The model showed its capability of the prediction of all test data.

Key Words : *dilatancy, surface degradation, stress transfer, discontinuities*

1. INTRODUCTION

The presence of cracks in concrete material can dramatically affect its mechanical behavior by providing planes of weakness across which frictional sliding can occur. Thus, the precise account of the behavior of concete discontinuities requires a realistic model as well as adequate mechanism for the behavior of discontinuities. Because of the natural process involved in their creation, concrete discontinuities are inherently rough and contact frequently takes place over relatively large portion of the available contact surface. This roughness involves the interaction of not only the aggregate - mortar contact but also the likelihood of mortar - mortar contact. Moreover, the asperity surfaces which are responsible for the dilatancy have finite strength and,depending upon the severity of stresses and the amount of sliding, will degrade and affect a change in the subsequent discontinuity behavior.

Since, it has been recognized that cracks in concrete have a significant effect on the mechanical response of concrete, there have been various attempts for both experimental investigation and analytical modeling aimed at representing cracked concrete for nonlinear analysis of concrete structures. Fenwick and Paulay[1], Houde and Mirza[2], and Paulay and Loeber[3] carried out the tests keeping the crack width constant by adjusting the magnitude of the external force during tesing to simplify the complex nature of the problem. The objective of these investigations was to experimentally examine the influence of the crack width, aggregate size, concrete properties, shape of specimens and loading history. In the experiments of Mattock[4], attention has been directed to the ultimate shear capacity. Millard and Johson[5] conducted direct shear tests using precracked concrete specimens restrained by embedded reinforcement, choosing a wide variety of test parameters such as initial crack width, axial stresses normal to the crack surface, and number and sectional areas of reinforcing bars.

On the other hand, quantitative description of the discontinuities with dilatancy is complex and many constitutive models have been developed. Bazant and Gambarova[6] constructed nonlinear equations to describe the complicated shear behavior. In their model, the model parameters are obtained by optimizing the fits of Paulay and Loeber's experiments[3] taking into account the influence of the maximum size of aggregate and concrete strength. Yoshikawa, Wu, and Tanabe[7] proposed a path independent model which clearly classifies the shear transfer phenomenon into four independent components, that is, interface shear stiffness, crack dilatancy, frictional contact and confining stiffness.

In addition to the previous macroscopic models, some microscopic physical models are also proposed. Walraven and Reinhardt[8] idealized the crack surface as a set of circular aggregates. The aggregates and surrounding mortar were modeled to be rigid-plastic bodies, where the effect of aggregate grading was considered. Bazant and Gambarova[9] introduced the microplane model which assumed the multi-directional uniaxial stress

* Member of JSCE, Dr. Eng., Nagoya University (Assist. Prof., Saitama University)
** Member of JSCE, Dr. Eng. Nagoya University (Research Associate, Kumamoto University)
*** Member of JSCE, Dr. Eng., Professor, Nagoya University (Nagoya 464, Japan)

distributions on the isotropically arranged microplane in the crack band. Li and Maekawa[10] introduced the contact density model, in which a few simple assumptions such as perfect elasic-plastic contact stress without any anisotropy or deteriorations due to contact fracturing were made. Later, Bujadham, Fujiyoshi and Maekawa[11], Bujadham and Maekawa[12)~14)], proposed the so called universal model which is devised based upon the framework of the contact density model[10] but with more realistic assumptions of anisotropic property of contact stress and deterioration of contact forces in order to consider the material nonlinearities. However, it has been assumed that all contacts with different orientations have the same behavior and the surface degradatin of the crack surface is not involved[10)~14)]. It can be noticed that a methodology which can involve all possible contacts, material as well as geometrical nonlinearities, surface degradation until crushing of the contact zone and dilatancy is necessary.

In the present study, a new physically motivated constitutive model for the behavior of concrete discontinuities with surface degradation, dilatancy and material nonlinearities is proposed. Both plastic and fracture deformations with the accumulated damage are formulated at the microlovel. By paying attention to the detailed contact mechanisms both for the contact between mortar and mortar and that between aggregate and mortar, the total deformation are assumed to be due to the aggregate intrelock and the fracture of mortar surface. The fracture of mortar is expressed by the degradation of the original asperity of the surface due to the current accumulated damage. Morevore, to simulate all sorts of nonlinearities, two independent hyperbolic surfaces which have Mohr-Coulomb surface as an asymptotic surfaces for both the plastic potential and the yield function are defined in stress space. The basic material parameters;cohesion, internal friction angle, dilatancy angle and tensile strength are varied according to the accumulated damage. Finally, several paths are considered to evaluate the capability of proposed model. The model is amenable to implementation in numerical procedure such as finite element computre programing.

2. THEORETICAL APPROACH OF THE PROPOSED MODEL

As shown in **Fig.1**, the cracked concrete is idealized to have plastic-fracture zone around the crack surfaces while the remaining part is assumed to behave as an elastic material. Furthermore, the geometry of the crack surfaces is idealized to consider both the aggregate interlock and the

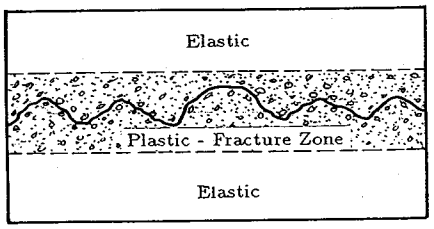

Fig.1 Idealized Concrete Material

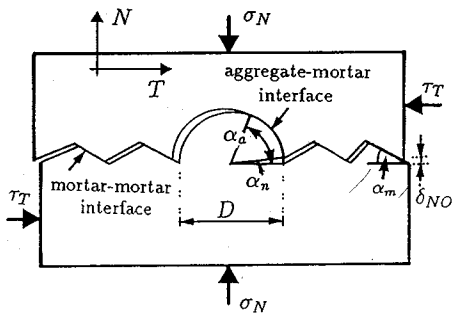

Fig.2 The Notations of Asperity Angles

fracture of mortar. To simulate the fracture of mortar, the crack surfaces are assumed to have sawtooth asperities as shown in **Fig.2**. Moreover, the phenomenon of aggregate interlock is introduced by considering circular sawtooth asperities as shown in **Fig.2**. In the present study, the analysis is focused at the crack interfaces where the plastic and fracture deformations are likely to occur.

(1) Surface Degradation

The concept of surface degradation is used to distinguish the geometrical nonlinearities of the contact zone. As shown in **Fig.2**, the asperity angles α_m and α_a for both mortar-mortar and aggregate-mortar interfaces have been tentatively expressed in terms of damage parameter ω as follows

$$\alpha_m = F_1(\omega) = \alpha_o \quad \exp(-a\omega) \qquad \cdots\cdots(1)$$

$$\left.\begin{aligned} \alpha_a = F_2(\omega) &= \alpha_n + \left(\frac{\pi}{2} - \alpha_n\right)\sqrt{2\omega - \omega^2} \quad \omega \le 1 \\ \alpha_a = F_2(\omega) &= \frac{\pi}{2} \qquad\qquad\qquad\qquad\quad \omega > 1 \end{aligned}\right\} \qquad \cdots\cdots(2)$$

where α_m and α_a are the current asperity angles at mortar-moter and aggregate-mortar interfaces, α_o is the initial asperity surface angle (α_m, α_a and α_o are in radian), 'a' is the material degradation parameter. Parameter 'a' reflects how repidly the asperity surfaces deteriorate. High and low values of the material parameter 'a' correspond to brittle (i.e. weak) and very resistant asperities, respectively. In this study, the values of $\alpha_o = 8° \sim 14°$(α_o should be used in radian) and 'a'$=1.0$ are selected

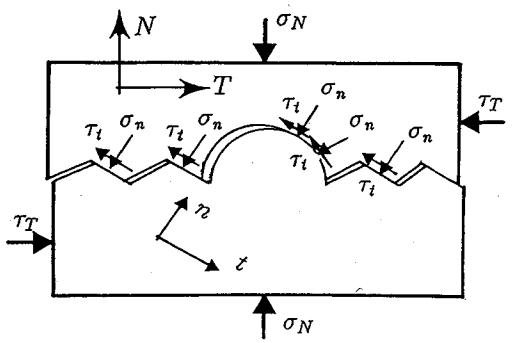

Fig.3 Macroscopic and Microscopic Stresses

to obtain a reasonable agreement with the test data. α_n is the initial asperity angle of aggregate-mortar interface due to crack opening which can be estimated as follows :

$$\alpha_n = 2\frac{\delta_{NO}}{D} \quad \cdots\cdots(3)$$

δ_{NO} is the initial crack opening and 'D' is the maximum aggregate size (refer to **Fig.2**). In Eq.(3), α_n is also in radian. As can be noticed in Eq.(3), δ_{NO} should be very small, i.e. $\delta_{NO} \ll D$. This fact is quit natural since in the engineering point of view the crack width should be as small as possible. In the current paper, the proposed model deals with the cases in which the crack width will be either constant or continuously open. However, the cases in which the crack width will open in some cracks and it closes under certain conditions will be precisely discussed in the next work for the cyclic behavior.

(2) The Relation Between Micro and Macro Variables

Plastic deformation on the asperity surfaces is defined with respect to the asperity reference system (n, t) as shown in **Fig.3**. The (n, t) reference system evolves with asperity degradation as the plastic deformation occurs. The evolution includes rotation of the (n, t) system with respect to the fixed (N, T) reference system as shown in **Fig.3**. The macroscopic normal and shear stresses (σ_N, τ_T) for both aggregate-mortar and mortar-mortar interfaces, can be fully transformed into asperity stresses (σ_n, τ_t) as shown in **Fig.3**. The transformation must account the degradation of the asperity angles. For a given instant of loading, both macroscopic displacements and stresses can be transformed into asperity displacements and stresses as follows

For Mortar-Mortar Interface :

$$\begin{Bmatrix}\sigma_n\\ \tau_t\end{Bmatrix} = \begin{bmatrix}\cos^2\alpha_m & 2\sin\alpha_m\cos\alpha_m\\ -\sin\alpha_m\cos\alpha_m & \cos^2\alpha_m-\sin^2\alpha_m\end{bmatrix} \begin{Bmatrix}\sigma_N\\ \tau_T\end{Bmatrix}_{(m-m)} \quad \cdots\cdots(4)$$

$$\begin{Bmatrix}\delta_n\\ \delta_t\end{Bmatrix} = \begin{bmatrix}\cos\alpha_m & \sin\alpha_m\\ -\sin\alpha_m & \cos\alpha_m\end{bmatrix} \begin{Bmatrix}\delta_N\\ \delta_T\end{Bmatrix} \quad \cdots\cdots(5)$$

For Aggergate-Mortar Interface :

$$\begin{Bmatrix}\delta_n\\ \delta_t\end{Bmatrix}_i = \begin{bmatrix}\sin\alpha_i & \cos\alpha_i\\ -\cos\alpha_i & \sin\alpha_i\end{bmatrix} \begin{Bmatrix}\delta_N\\ \delta_T\end{Bmatrix} \quad \cdots\cdots(6)$$

$$\begin{Bmatrix}\sigma_n\\ \tau_t\end{Bmatrix}_i = \begin{bmatrix}\sin^2\alpha_i & 2\sin\alpha_i\cos\alpha_i\\ -\sin\alpha_i\cos\alpha_i & \sin^2\alpha_i-\cos^2\alpha_i\end{bmatrix} \begin{Bmatrix}\sigma_N\\ \tau_T\end{Bmatrix}_{(a-m)} \quad \cdots\cdots(7)$$

where $\alpha_i = \alpha_n \sim \alpha_a$ (i.e. before the beginning of the degradation of aggregate-mortar contact, $\alpha_i = \alpha_n$. However, when the degradation starts, α_i represents all angles between α_n and the current angle of α_a which can be calculated from Eq.(2)), $(m-m)$ and $(a-m)$ refer to both mortar-mortar and aggregate-mortar contacts.

(3) Microscopic Plastic-Fracture Formulation

The present formulation follows the basic concepts of the theory of plasticity. These formulation will be carried out in the (n, t) reference system. The subsequent yield surface is assumed to change its size depending on the damage accumulated at each crack interface, i.e., the failure surface f is a function of the damage parameter ω (W^{pf}) as follows

$$f = f(\sigma_i, \omega(W^{pf})) = 0 \qquad i = n, t \quad \cdots\cdots(8)$$

An independent function, i.e., plastic potential function g is defined as follows

$$g = g(\sigma_i, \omega(W^{pf})) = 0 \qquad i = n, t \quad \cdots\cdots(9)$$

where σ_i denotes the asperity stresses (σ_n, τ_t) and ω is the accumulated damage which is a function of the accumulated plastic-fracture work W^{pf} after initial failure.

The first postulate of the plasticity theory is the decomposition of the incremental displacement ($\delta_j, j = n$ and t) into an elastic δ_j^e and plastic-fracture δ_j^{pf} portions :

$$d\delta_j = d\delta_j^e + d\delta_j^{pf} \qquad j = n, t \quad \cdots\cdots(10)$$

where δ_j denotes the asperity displacements (δ_n, δ_t). Another postulate is that only the elastic displacements induce stresses. Using Hook's law, this postulate can be expressed by

$$d\sigma_i = k_{ij}^e d\delta_j^e = k_{ij}^e (d\delta_j - d\delta_j^{pf}) \quad \cdots\cdots(11)$$

where k_{ij}^e is the microscopic elastic stiffness tensor for the interface. The value of k_{ij}^e can be obtained from the corresponding macroscopic one through

stress-displacement transformation matrices in Eqs.(4)~(7). In the non-associated flow rule, the plastic-fracture displacement increments can be obtained from the plastic potential as follows :

$$d\delta_j^{pf}=d\lambda\frac{\partial g}{\partial\sigma_j} \quad \cdots\cdots (12)$$

where $d\lambda$ is non-negative scalar which can be determined from the consistency condition during loading. The consistency condition $df=0$ can be expressed as :

$$df=\frac{\partial f}{\partial\sigma_i}d\sigma_i+\frac{\partial f}{\partial W^{pf}}dW^{pf}=0 \quad \cdots\cdots (13)$$

where dW^{pf} can be written as follows :

$$dW^{pf}=\sigma_i d\delta_i^{pf} \quad \cdots\cdots (14)$$

Substituting Eqs.(11), (12) and (14) into Eq.(13) and solving for $d\lambda$, the followig results can be obtained

$$d\lambda=\frac{\dfrac{\partial f}{\partial\sigma_i}k_{ij}^e\,d\delta_j}{\dfrac{\partial f}{\partial\sigma_m}k_{mn}^e\dfrac{\partial g}{\partial\sigma_n}+h} \quad \cdots\cdots (15)$$

with the definition of

$$h=-\frac{\partial f}{\partial W^{pf}}\sigma_i\frac{\partial g}{\partial\sigma_i} \quad \cdots\cdots (16)$$

Finally, by substituting Eqs.(15) and (12) into Eq.(11), the elasto-plastic-fracture stiffness matrix for each interface can be written in the following form:

$$k_{ij}^{epf}=k_{ij}^e-\frac{k_{iq}^e\dfrac{\partial f}{\partial\sigma_p}\dfrac{\partial g}{\partial\sigma_q}k_{pj}^e}{\dfrac{\partial f}{\partial\sigma_m}k_{mn}^e\dfrac{\partial g}{\partial\sigma_n}+h} \quad \cdots\cdots (17)$$

Note that $\partial f/\partial W^{pf}$ in Eqs.(13) and (16) will have a negative value for the hardening behavior and a positive value for the softening behavior. In Eqs.(11)~(17), the lower-case subscriptsr refer to the asperity reference system (n, t). Moreover, the repeated lower-case subscripts indicate summation over n and t.

(4) Modified Mohr-Coulomb Potential and Failure Surfaces

The subsequent yield surface is defined as a hyperbolic surface as follows :

$$f=\tau_t^2-(C^*-\sigma_n\tan\phi^*)^2+(C^*-\chi^*\tan\phi^*)^2 \quad \cdots\cdots (18)$$

Besides, a similar expression for the plastic potential function is assumed as follows

$$g=\tau_t^2-(C^*-\sigma_n\tan\psi^*)^2+(C^*-\chi^*\tan\psi^*)^2 \quad \cdots\cdots (19)$$

The subsequent yield surface in Eq.(18) and the potential function in Eq.(19) are shown in **Fig.4**, and it may be recognized that the surfaces have Mohr-Coulomb surface as their asymptotic surface.

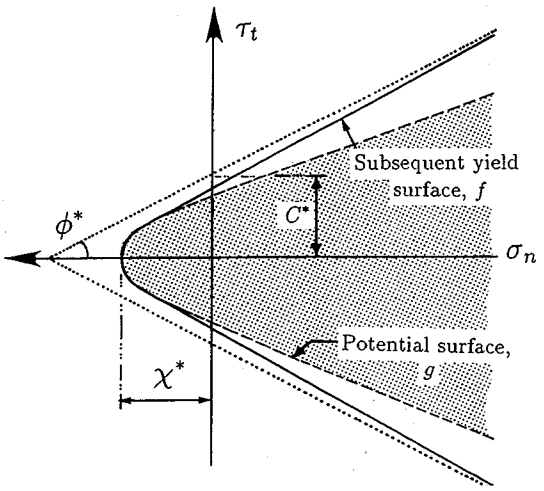

Fig.4 Hyperbolic Yield and Potential Surfaces

The notations ϕ^*, C^*, χ^* and ψ^* are the mobilized friction angle, the cohesion, the tensile strength (tension cutoff) and the dilatancy angle, which are not constant but depend on the plastic-fracture history through the damage parameter ω. All of these material parameters are used to consider the material nonlinearities. Referring to the previous work of Wu and Tanabe[15], the possible relations are suggested to be as follows :

$$C^*=C_o\exp[-(m\omega)^2] \quad \cdots\cdots (20)$$

$$\left.\begin{array}{ll}\phi^*=\phi_o+(\phi-\phi_o)\sqrt{2\omega-\omega^2} & \omega\le 1\\ \phi^*=\phi & \omega>1\end{array}\right\} \cdots (21)$$

$$\left.\begin{array}{ll}\chi^*=f_t(1-\omega) & \omega\le 1\\ \chi^*=0 & \omega>1\end{array}\right\} \cdots\cdots (22)$$

In the same manner, the mobilized dilatancy angle is defined as follows :

$$\left.\begin{array}{ll}\psi^*=\psi_o+(\psi-\psi_o)\sqrt{2\omega-\omega^2} & \omega\le 1\\ \psi^*=\psi & \omega>1\end{array}\right\} \cdots (23)$$

where m is a material parameter, C_o, f_t, ϕ_o, ϕ and ψ are the initial cohesion, the tensile strength, the initial friction angle, the final friction angle, and the final dilatancy angle, respectively. All these relations are shown in **Fig.5**. With a defined mobilized dilatancy angle ψ. It is noted that for $\psi=\phi$, we have $f=g$ and the classical associated flow rule is recovered. It is very important here to note that the initial material parameters for both aggregate-mortar and mortar-mortar contacts are same. Theerefore, the initial yield surfaces for both contacts are also same. However, since the material parameters at both contacts, which govern the evolution of the subsequent yield surface, vary

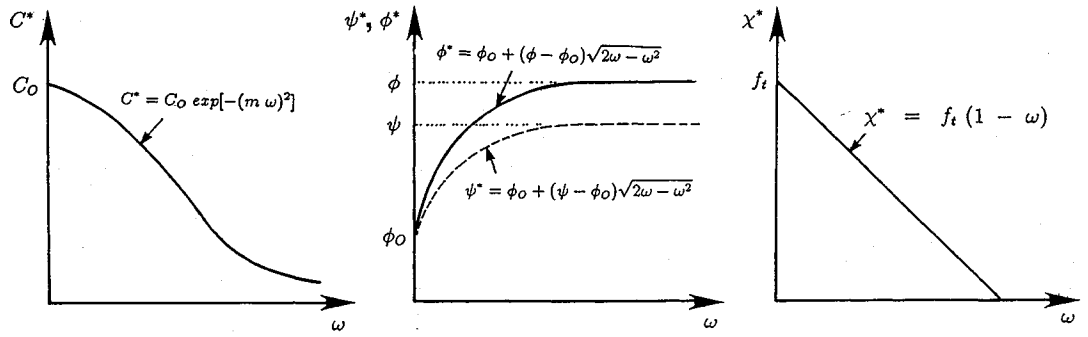

Fig.5 Possible Relations of $C^*-\omega$, $\phi^*-\omega$, $\psi^*-\omega$ and $\chi^*-\omega$

independently according to the accumulated damage, the subsequent yield surface is completely different at both contacts during loading.

From Eq.(18), the subsequent yield surface is expressed in terms of C^*, ϕ^* and χ^* parameters. Moreover, from Eqs.(20), (21) and (22), these parameters are assumed to be unique function of the damage parameter ω and defined to characterize the shape and size of the yield surface. Therefore, the function $\partial f/\partial W^{pf}$ in Eqs.(13) and (16) can be elaborated as follows :

$$\frac{\partial f}{\partial W^{pf}}=\left(\frac{\partial f}{\partial C^*}\frac{\partial C^*}{\partial \omega}+\frac{\partial f}{\partial \phi^*}\frac{\partial \phi^*}{\partial \omega}+\frac{\partial f}{\partial \chi^*}\frac{\partial \chi^*}{\partial \omega}\right)\frac{\partial \omega}{\partial W^{pf}} \quad \cdots\cdots (24)$$

The damage parameter is linked with the accumulated plastic-fracture work as follows :

$$\omega=\beta\int dW^{pf} \quad \cdots\cdots (25)$$

where β is a material parameter.

(5) Macroscopic Stress-Displacement Relationship

Based on Voigt's model, the average stress increment for two kinds of contacts can be expressed as follows :

$$d\bar{\sigma}_{ij}=\frac{1}{S}\left(\int_{S_{a-m}} d\sigma_{ij(a-m)}ds+\int_{S_{m-m}} d\sigma_{ij(m-m)}ds\right) \quad \cdots\cdots (26)$$

Eq.26 yields to the following equation :

$$d\bar{\sigma}_{ij}=\frac{S_{a-m}}{S}d\bar{\sigma}_{ij(a-m)}+\frac{S_{m-m}}{S}d\bar{\sigma}_{ij(m-m)} \quad \cdots\cdots (27)$$

Considering the case of homogenous strain state (i.e., $\bar{\varepsilon}_{ij}=\bar{\varepsilon}_{ij(a-m)}=\bar{\varepsilon}_{ij(m-m)}$) with the help of Eq.(27), the incremental stress-displacement relation is given as follows:

$$d\bar{\sigma}_i=\left[\eta K^{epf}_{ij(a-m)}+(1-\eta)K^{epf}_{ij(m-m)}\right]d\delta_j$$
$$=K^{epf}_{ij(c)}d\delta_j \quad \cdots\cdots (28)$$

where η is the percentage of the area of aggergate at interface with respect to the total surface area of crack. Both S_{a-m} and S_{m-m} denote the surface areas of aggregate-mortar and mortar-mortar interfaces. $K^{epf}_{ij(c)}$ $K^{epf}_{ij(a-m)}$ and $K^{epf}_{ij(m-m)}$ are the macroscopic elasto-plastic-fracture stiffiness matrices for concrete, aggregate-mortar, and mortar-mortar interfaces, respectively. The notations $(m-m)$ and $(a-m)$ refer to both mortar-mortar and aggregate-mortar interfaces. In this study, the elastic macrostiffiness of mortar-mortar interface is assumed to be linear with that of concrete as follows :

$$K^e_{ij(m-m)}=RK^e_{ij(c)} \quad \cdots\cdots (29)$$

in which $K^e_{ij(c)}$ is the elastic stiffness matrix for concrete at the crack interface. The value of 'R' should be obtained experimentally. However, this value will be obtained to achieve a reasonable agreement with the test data. The elastic stress-displacement relation for concrete in Eq.(28) in a matrix form is given as follows :

$$\begin{Bmatrix} d\bar{\sigma}_N \\ d\bar{\tau}_T \end{Bmatrix}=\begin{bmatrix} K_N & 0 \\ 0 & K_T \end{bmatrix}\begin{Bmatrix} d\delta_N \\ d\delta_T \end{Bmatrix},\quad K^e_{ij}(c)=\begin{bmatrix} K_N & 0 \\ 0 & K_T \end{bmatrix} \quad \cdots\cdots (30)$$

where K_N and K_T are the initial normal and shear stiffnesses of the contact zone. Since the elastic behavior in any reference system is independent of plastic deformation on the asperity surfaces, the above relation can always be transformed into (n,t) system.

3. SENSITIVITY ANALYSIS OF THE MODEL

To see the applicability of the proposed plastic - fracture model for stress transfer at concrete discontinuities, the sensitivity of the model for different model parameters are examined. As shown in **Fig.6** (a and c), the model exhibits more softening with the increase of the values of β_m and β_a. Moreover, as shown in **Fig.6** (b and d), with the increase of those two material parameters, i.e. β_m and β_a, more surface degradation is found. In

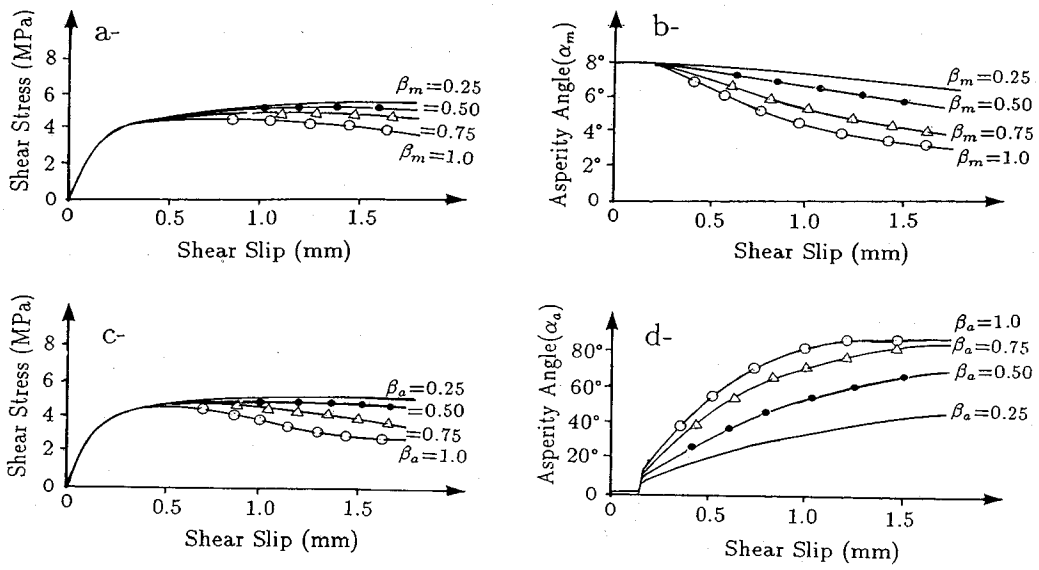

Fig.6 Effect of The Material Parameters β_m and β_a

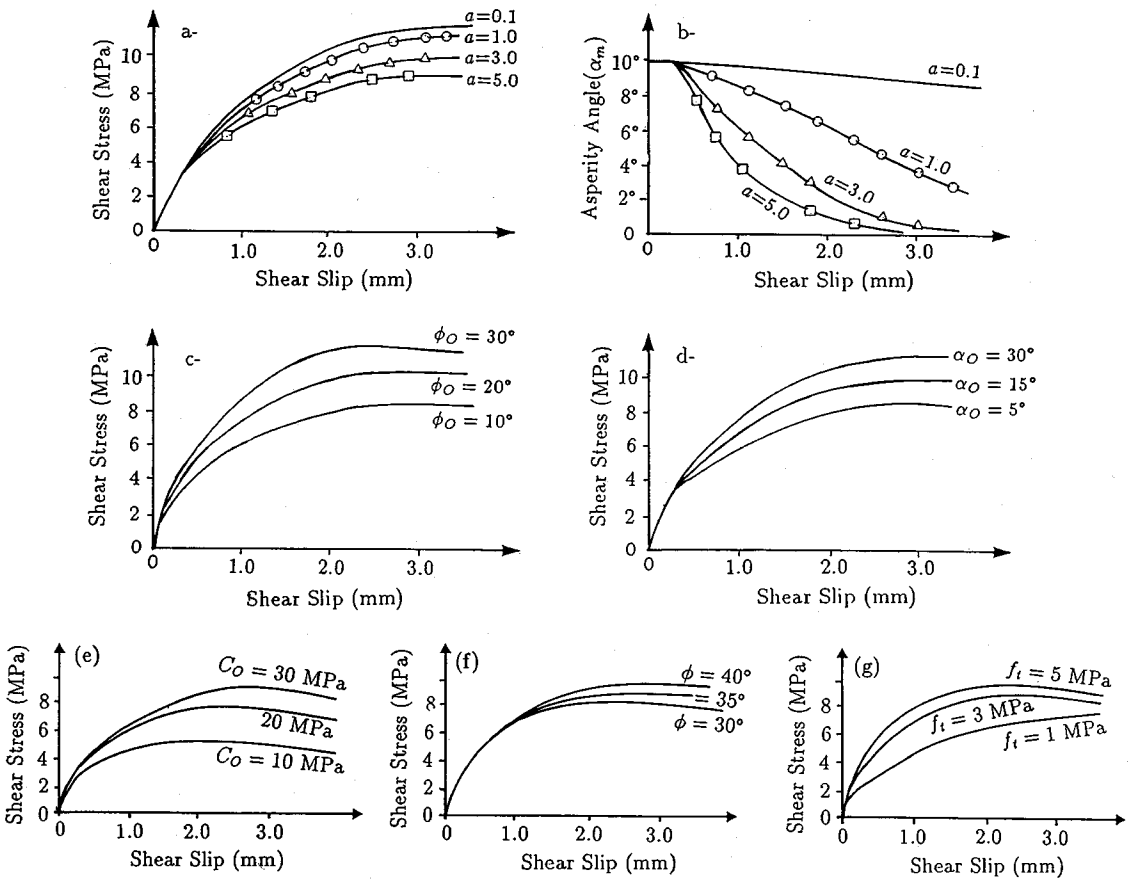

Fig.7 Effect of The Material Parameters a, ϕ_o, α_o, C_o, ϕ and f_t

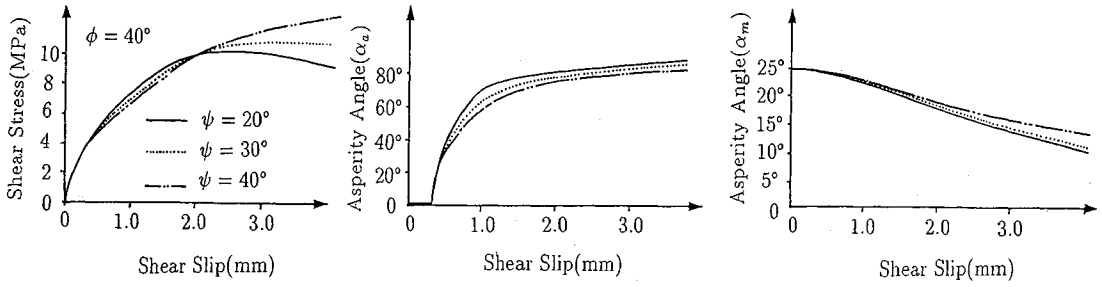

Fig.8 Effect of Dilatancy ϕ

Table 1 Estimation of the Material Parameters

Material Parameter	Estimated Value	Material Parameter	Estimated Value
C_O	$f_c'/(1.0 \sim 1.45)$	f_t	$f_c'/12$
a	1.0	m	1.0
η	0.50	R	0.90
ϕ	40°	α_O	7° ~ 12°
ϕ_O	20° (constant crack width) 7° (variable crack width)	β_m β_a	1.0 0.70 ~ 1.0

Fig.6, the material parameters are assumed to be as : C_O=15MPa, ϕ=40°, ϕ_O=7°, Ψ=30°, f_t=3.60 MPa, a=1.0, η=0.40 and α_O=8°. Also, when the effect of β_m is investigated, the value of β_a=0.40 is assumed. On the other hand, when the effect of β_a is considered, the value of β_m=1.0 is assumed. All numerical analysis have been made under the condition of constant crack width.

From **Fig.7** (a and b), as the value of the material parameter 'a' in Eq.(1) increases, more degradation of the asperity angle as well less shear resistance are observed. As shown in **Fig.7** (c, d, e, f and g), the shear resistance increases with the increase of initial friction angle ϕ_O, initial asperity angle α_O final friction angle ϕ and the tensile strength f_t. In **Fig.7**, the material parameters are taken as : C_O=20 MPa, ϕ=40°, ϕ_O=10°, ψ=30°, f_t =3.0 MPa, a=0.10, η=0.40 and α_O=10°. All numerical analysis have been made under the condition of constant crack width.

Fig.8, shows the effect of dilatancy angle. It can be seen that, as the final dilatancy angle decreases, a more degradation of the asperity angles is observed. The degradation of the asperity angles yield to more horizontal plateau of shear resistance. However, the plastic plateau is one of the main features of the observed experimental data. All the material parameters used in **Fig.7** are also used in **Fig.8**.

4. ESTIMATION OF THE MODEL PARAMETERS

As can be seen in the previous Section, a great effort has been made to estimate the model parameters. It is noticed that the relation between the model parameters and the uniaxial compressive strength is not straigit forward. However, based on the fitting of the experimental data, the model parameters can be predicted and listed in **Table 1.** The valuse of the initial stiffnesses, i.e. K_N and K_T for concrete are estimated based on the experimental results of ref.7). In ref.7), the value of δ_{T1} is the frictional slip where the interfaces will be in full contact. Before reaching the value of δ_{T1}, the shear stiffness is considered to be nonlinear as follows :

$$K_T = K_{IST}\,\mathrm{sech}^2\left\{\frac{K_O}{\tau_u}(\delta_T - \delta_{T1})\right\} \cdots\cdots\cdots (31)$$

where

$$\delta_{T1} = 1.42\left(\frac{D_a}{16}\right)^{-1.20}(\delta_{NO})^{1.31},$$

$$K_{IST} = 8.60\left(\frac{f_c'}{25}\right)^{0.6}(\delta_{NO})^{-0.96}$$

$$K_O = K_{IST}(1+q), \quad q = \tanh\left(\frac{K_O}{\tau_u}\delta_{T1}\right),$$

$$\tau_u = \frac{0.01}{0.01+\left(\frac{\delta_{NO}}{D_a}\right)^2}\tau_O, \quad \tau_O = (0.20 \sim 0.30) f_c'$$

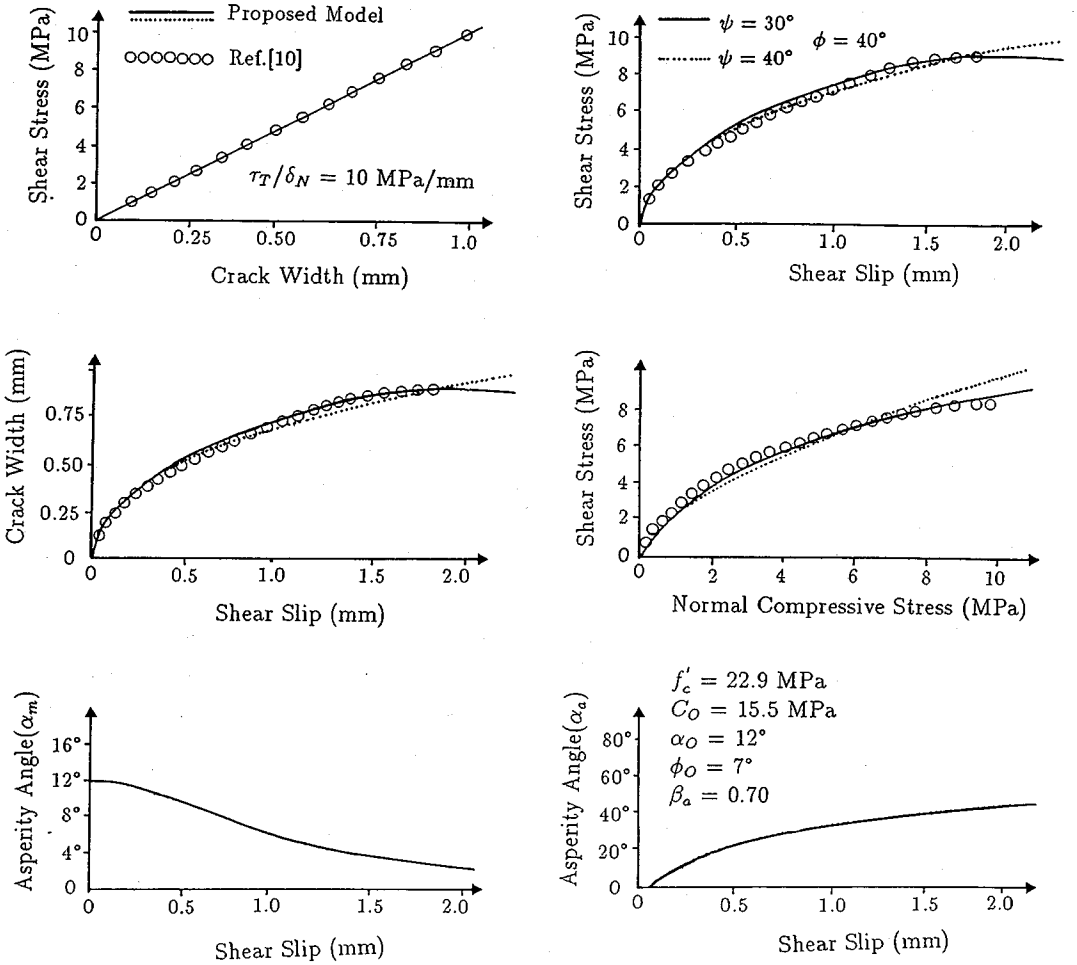

Fig.9 Path (1) Comparison with The Experimental Data of Ref. 10)

After reaching the value of δ_{T1}, the shear stiffness reaches its maximum value and it will be kept constant with the following value

$$K_T = K_{IST} \quad \cdots\cdots (32)$$

In the previous equations, δ_{NO} is the initial crack width. In Eq.(31) and Eq.(32), the units of f'_c is in MPa, while the units of D_a and δ_{NO} are in *mn*.

The normal stiffness is reported experimentally by Yoshikawa et al.[7] to be as follows:

$$K_N = 0.0072 f'_c (\delta_N - \beta_d \delta_T)^{-1.878} \quad \cdots\cdots (33)$$

in which β_d is the dilatancy ratio. In the current study, since there is no initial shear slip before loading, the normal stiffness K_N is estimated using Eq.(33) at $\delta_T = 0$ and $\delta_N = \delta_{NO}$. Then, the estimated value was kept constant in all analysis.

5. VERIFICATION OF THE PROPOSED MODEL

To examine the capability of the proposed model, the results of several experimental data with different paths are compared with the results of the proposed model. The different paths include the following cases :

Path(1)..shear stress/crack opening=constant.
Path(2)..constant crack width.
Path(3)..constant crack width with variable concrete strength.
Path(4)..constant applied compressive strength.

In the beginning, the model parameters are estimated according to the explanation in the previous section. Finally, the model results using the estimated paramenters are compared with the available experimental and numerical data. As will be seen in the next discussion, a good agreement with the experimental work is obtained. The comparison are observed as follow :

Path (1) Shear Stress/Crack Opening= Constant.

In this path, the experiment of Li and Maekawa[10], in which the ratio of shear stress to crack opening is kept constant at a value of 10

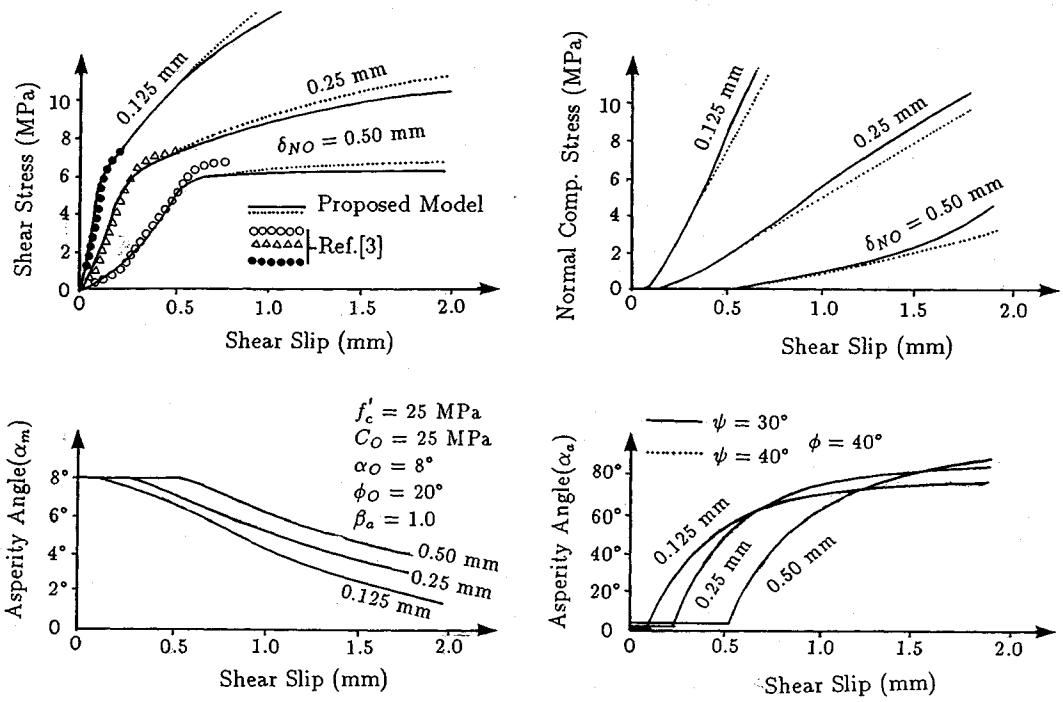

Fig.10 Path (2) Comparison with The Experimental Data of Ref. 3)

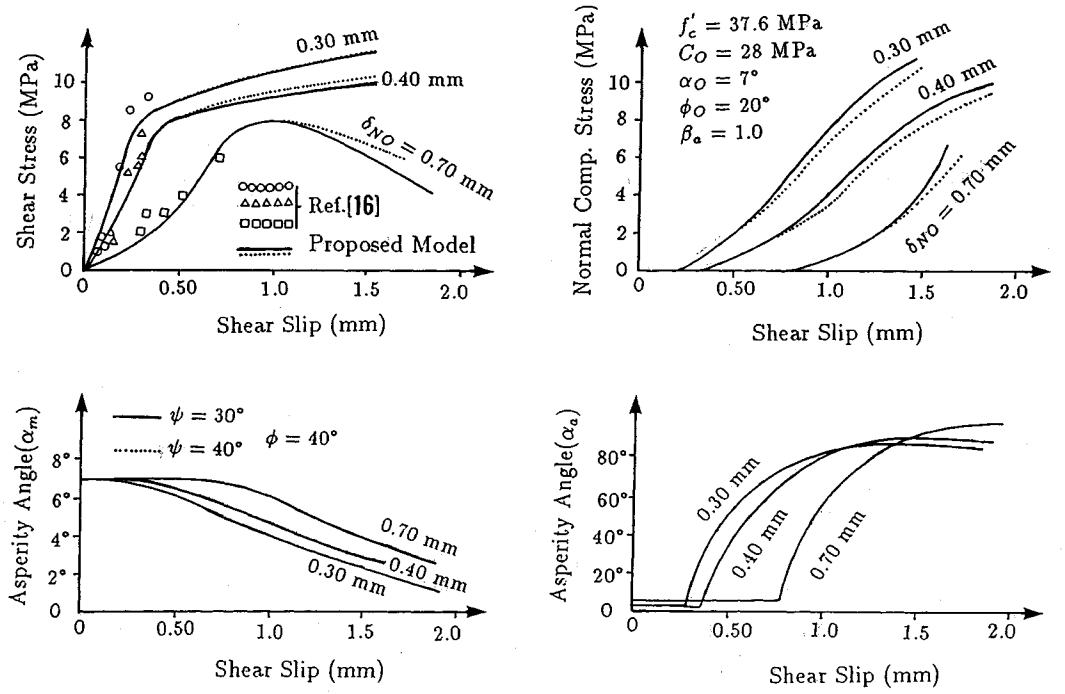

Fig.11 Path (2) Comparison with The Experimental Data of Ref.16)

MPa/*mm*, is examined. **Fig.9** shows the comparsion between the model results and the experiments as well as the surface degradation during loading. As can be seen, a good agreement with the test data is observed. From **Fig.9**, it can be noticed that a horizontal plateau, where the ultimate shear strength takes place, is also found without specifying its value. From **Fig.9**, it can be easily noticed

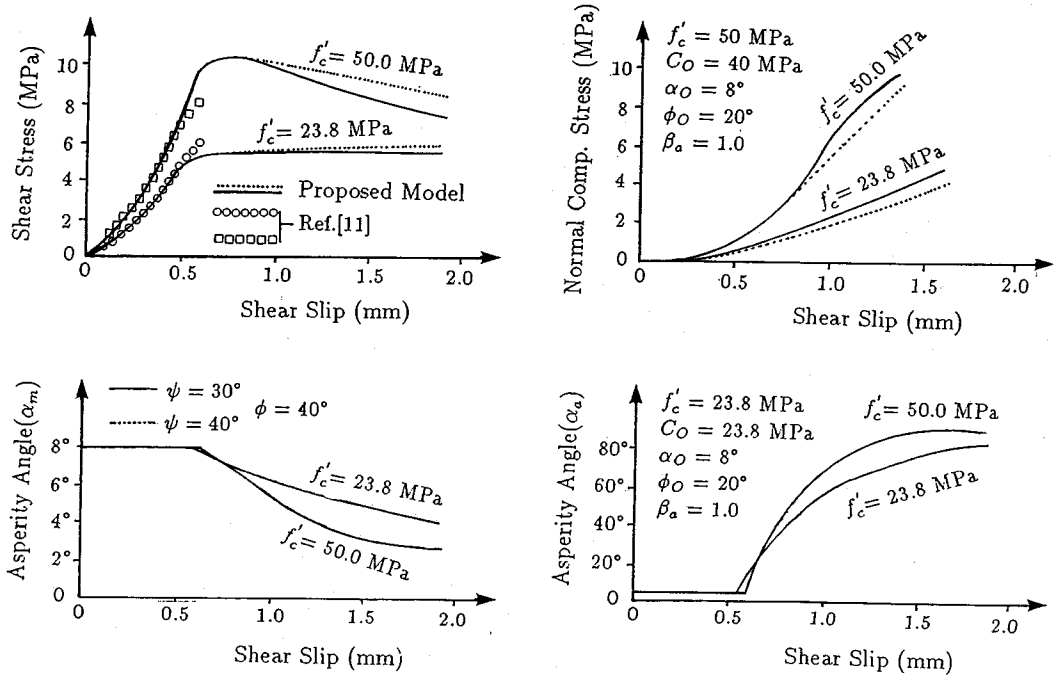

Fig.12 Path (3) Comparison with The Experimental Data of Ref.11)

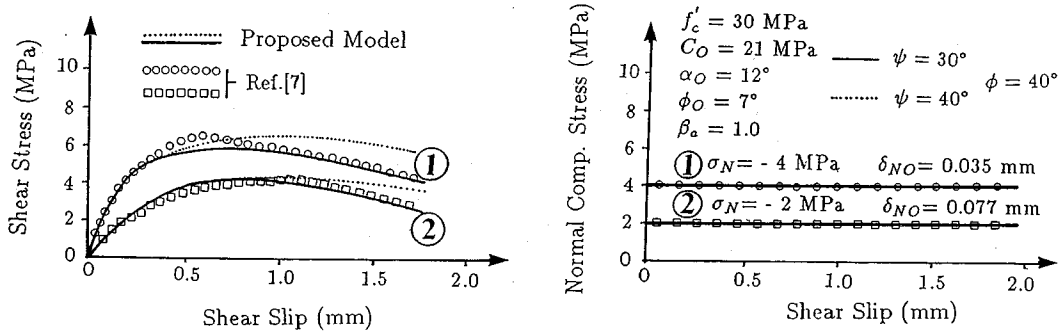

Fig.13 Path (4) Comparison with The Numerical Data of Ref.7)

that both the associated and the non-associated flow rule give a good prediction of the experimental data. However, with the use of the non-associated flow rule, better results at the final stages of loading are obtained. In the analytical results, the initial normal and shear stiffnesses are measured from the experimental data since there is no information about the initial crack opening.

Path (2) Constant Crack Width.

In this path, the experimental work of both Paulay and Loeber[3] and Reinhardt and Walraven[16] are investigated. In these experiments[3),6)], different constant crack widths are considered. As can be seen, the model can predict the experimental work with a certain accuracy using either the associated or the non-associated flow rule. From **Figs.10** and **11**, it can be noticed that as the crack width increases, less shear resistance, more horizontal plateau and less surface degradation are observed. Also, from **Figs.10** and **11**, with the use of the non-associated flow rule, more degradation of the shear resistance is obtained, while more normal compressive stresses are observed.

Path (3) Constant Crack Width with Variable Concrete Strength.

In this path, as shown in **Fig.12**, the experimental work of Bujadham, Fujiyoshi and Maekawa[11] is compared with the model results. In the experiments, the crack width was kept constant with a value of δ_{NO}=0.50 mm. As shown in **Fig.12**, naturally, it is observed that as the concrete strength increases, the shear capacity increases. It is also foud that the surface degradation starts earlier in the case of smaller concrete strength. On

the other hand, in the case of higher concrete strength, although later surface degradation is found, a more rapid degradation is observed.

Path (4) Constant Normal Compressive Stress.

In this path, as shown in **Fig.13**, the numerical results of the proposed model by Yoshikawa, Wu,and Tanabe[7], are compared with the model results. As can be seen, a good agreement is observed. This shows that the proposed model is capable of predicting the behavior in all possible paths. As shown in **Fig.13**, more accurate prediction of the results of ref.7) is obtained with the use of the non-associated flow rule.

6. CONCLUSIONS

A general constitutive law for shear stress transfer mechanism is proposed. A major feature of the proposed model is the development of an explicit relation between the increments of stresses and relative discontinuity displacements at all possible interfaces across the crack. Such a relation can be implemented in the FEM computer codes and should render more realistic and reliable than those currently performed with more simple idealization which neglect dilatancy and surface dagradation. The numerical calculations showed that the proposed model can predict with high accuracy the stress transfer problem for concrete discontinuities under the effect of all possible paths of loadings. However, it is considered that the present model has its great advantage to deal with more general problems such as the cyclic behavior and the time effect. These phenomena are under investigation now.

ACKNOWLEDGMENT

This paper is a part of the second author's Doctoral research work in the concrete laboratory of the Department of Civil Engrg., Nagoya University.

REFERENCES

1) Fenwick, R.C. and Paulay, T. : Mechanisms of Shear Resistance of Concrete Beams, Journal of Struct. Div., ASCE, Vol.94, No.10, pp.2325~2350, 1968.

2) Houde, J. and Mirza, M.S. : Investigation of Shear Transfer Across Cracks by Aggregate Interlock, Res. Report No.72~06, Ecole Polytechnique de Montreal, Canada, 1972.

3) Paulay,T. and Loeber, P.J. : Shear Transfer by Aggregate Interlock, Journal of America Concrete Inst., ACI, SP42, pp.1~15, 1974.

4) Mattock,A.H. : Cyclic Shear Transfer and Type of Interface, Journal of Struct. Div., ASCE, Vol.107, No.10, pp.1945~1964. 1981.

5) Millard, S.G. and Johneson, R.D. : Shear Transfer in Cracked Reinforced Concrete, Magazine of Concrete Research, Vol.17, No.130, pp.3~15, March, 1985.

6) Bazant, Z.P. and Gambarova, P. : Rough Cracks in Reinforced Concrete, Journal of Struct. Div., ASCE, Vol.106, No.4, pp.819~842, April, 1981.

7) Yoshikawa, H., Wu, Z.S. and Tanabe, T. : Analytical Model for Shear Slip of Cracked Concrete, Journal of Struct. Engrg., ASCE, Vol.15, No.4, pp.771~788, April, 1989.

8) Walraven, J.C. and Reinhardt, H.W. : Theory and Experiments on The Mechanical Behavior of Crack in Plain and Reinforced Concrete Subjected to Shear Loading, HERON, Vol.26, No.1A, 1981.

9) Bazant, Z.P. and Gambarova, P. : Crack Shear in Concrete : Crack Band Microplane Model, Journal of ASCE, Vol.110, No.9, pp.2015~2035, Sept. 1984.

10) Li, B. and Maekawa, K. : Stress Transfer Constitutive Equation for Cracked Plane of Concrete Based on the Contact Plane Density Function, Concrete Journal, JCI, Vol.26, No.1, pp.123~137, Jan. 1988. (in Japanese)

11) Bujadham, B., Fujiyoshi A. and Maekawa, K. : Crack Surface Asperity on Stress Transfer Mechanism, Proceeding of the Japan Concrete Institute, Vol.11, No.2, 1989.

12) Bujadham, B. and Maekawa, K. : Qualitative Studies on Mechanism of Stress Transfer Across Cracks in Concrete, Proceeding of the Japan Society of Civil Engineers, JSCE, No.451/V-17, pp.265~275, August, 1992.

13) Bujadham, B. and Maekawa, K. : The Universal Model for Stress Transfer Across Cracks in Concrete, Proceeding of the Japan Society of Civil Engineers, JSCE, No.451/V-17, pp.277~287, August, 1992.

14) Bujadham, B., Mishima, T. and Mackawa, K. : Verification of the Universal Stress Transfer Model, Proceeding of the Japan Society of Civil Engineers, JSCE, No.451/V-17, pp.289~300, Augsut, 1992.

15) Wu, Z.S. and Tanabe, T. : A Hardening-Softening Model of Concrete Subjected to Compressive Loading, Journal of Struct. Engrg., AIJ, Vol.36B, pp.153~162, 1990.

16) Reinhardt, H.W. and Walraven, J.C. : Cracks in Concrete Subjected to Shear, Journal of Structural Engineering, ASCE, Vol.108, No.1, pp.207~224, 1982.

17) Farahat, A.M. : Development of Concrete Models Based on the Micromechanics of Granular Material, Ph. D thesis, Nagoya University, March 1993.

(Received July 15, 1992)

ダイレイタンシー効果および表面損傷を考慮したコンクリート不連続面のモデル化

呉　智深・アハメド モハメド ファラハット・田辺忠顕

コンクリートの不連続面の挙動について，新たな構成モデルが提案された．不連続面での微視的な挙動を表現するために，骨材とモルタルの界面接触とモルタル間の接触による挙動を分離し個別に取り扱った．非線形挙動を解析には，塑性ポテンシャル面と降伏曲面の両者に対して漸近的なモールクーロン曲面を持つ２つの独立な双曲面を応力空間で定義した．そして，粘着力，内部摩擦角，ダイレイタンシー角，引張強度などは，損傷集積度に応じて変化させた．

土木学会出版案内

新刊案内

海岸工学用語集
「シソーラス付」「和英対照付」

A 5版　430頁
定価　2,000円
会員特価　1,800円
〒480円

フォース橋の100年
100 YEARS OF THE FORTH BRIDGE

B 5版　160頁
定価　5,000円
会員特価　4,500円
〒480円

橋　1991—1992
BRIDGES IN JAPAN

A 4版　158頁
定価　8,500円
〒480円

軟岩評価
—調査・設計・施工への適用—

B 5版　386頁
定価　6,000円
会員特価　5,400円
〒480円

BASIC Pascal C
による土木情報処理の基礎 II
サンプルプログラム収録　フロッピーディスク付(5inch)

B 5判　271頁
定価　3,800円
会員特価　3,400円
〒480円

土木學會誌　1992年6月号別冊増刊

エコ・シビルエンジニアリング読本

［第1章］
環境社会システム史
Part 1 Eco-Social Systems

［第2章］
自然生態系の保全・復元と創造をめざして
Part 2 Toward Preservation, Restoration, and Creation of the Ecosystem

［第3章］
物質循環・エネルギー循環のマネジメント
Part 3 Management of Material Recycling and Energy Conservation

［第4章］
世界に貢献する地球環境都市の構想
Part 4 The Eco-Polis in Global Society

A 4版　120頁
定価　2,000円
〒100円

お申込みは…社団法人　土木学会　刊行物販売係　〒160 東京都新宿区四谷1丁目無番地
☎ 03(3355)3441 内線144・145・146　郵便振替　東京6－16828

旧バージョン(Ver. 1.0)ご使用の皆様、お待たせいたしました。

未来設計企業
CRC

好評につき

新バージョン(Ver.2.0)

リリース開始!

任意形状臨界すべり面自動決定システム

Mr. 一番すべり Ver. 2.0

Mr. 一番すべりは、簡易**Janbu**法に基づき**任意形状**臨界すべり面位置を**自動的に探索**し、安全率を算定する斜面安定計算システムです。ご好評をいただいた本システムが、さらに充実した操作性、新機能を備えて新登場しました。

Ver. 2.0 新機能

- ◆計算対象すべり面制限機能(定義した部分をすべり面が必ず通過する)
- ◆必要抑止力の計算(任意の必要安全率に対して計算する)
- ◆臨界すべり面位置座標のファイル出力
- ◆既知すべり面のデータ入力による安全率の算定
- ◆外水面の導入(フィルダムなどの湛水斜面に対応)
- ◆結果のハードコピー機能
- ◆マウス誤操作時のやり直し機能

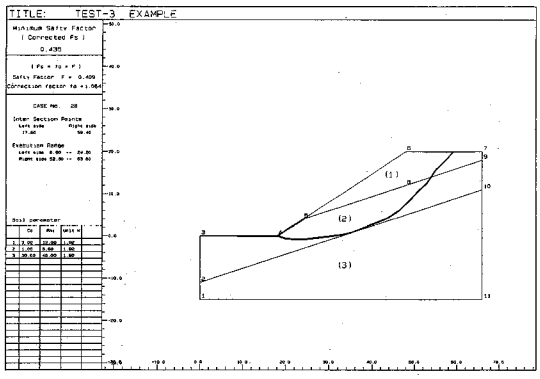

軟弱層をはさむ場合

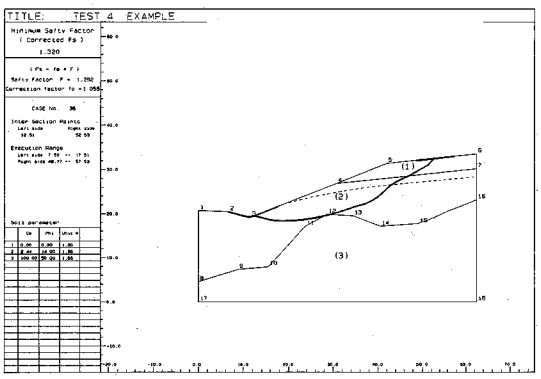

凸形基盤上の切土斜面

適応機種：NEC PC9801シリーズ

価　　格：50万円（税別）

(既にVer. 1.0をご使用の場合は、5万円で交換致します)

デモプログラム貸出中

あなた自身の手でご確認ください。

株式会社CRC総合研究所 西日本支社

〒541 大阪市中央区久太郎町4丁目1-3
(06) 241-4121 営業担当:岩 崎
(03)3665-9741 本社窓口:小 林

米国ITASCA（イタスカ）社開発の岩盤・地盤解析プログラム

未来設計企業 CRC

UDEC 3DEC

個別要素法(DEM)プログラム

個別要素法（離散要素法）は、1971年にDr.P.Cundallが発表した不連続体数値解析手法であり、岩盤や地盤をブロックや土粒子の要素の集合体と考え、個々の要素が隣接要素から受ける力により運動方程式にもとづき挙動する様子を時間差分式にて時刻繰返し計算する手法です。個別要素法は不連続力学の中心手法として位置づけられ、岩盤・地盤の崩落や安定性の解析、大深度地下空間、核廃棄物地下処理、鉱物資源開発等のプロジェクトおよび粒状体力学（粉体工学）の分野で有力な解析手段となっています。現在UDEC，3DECは全世界の研究機関・企業で標準コードとして広く使用されています。

オプション

■Barton-Bandisモデル

適用分野

- ●粒状物質の挙動解析
- ●鉱山採掘等　掘削解析
- ●地震応答解析
- ●ジョイント内流れ解析
  （浸透連成：UDEC）
- ●核廃棄物の熱応力解析
  （熱連成：UDEC）

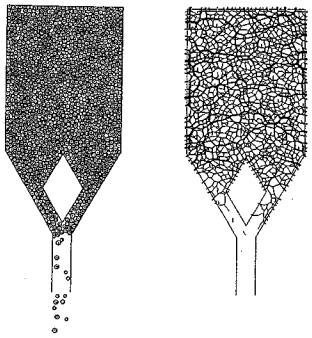

ホッパー内粒状体挙動解析

亀裂性岩盤の3次元掘削解析

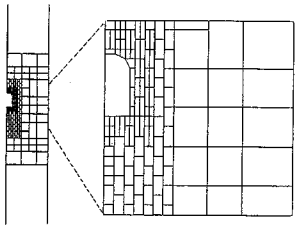

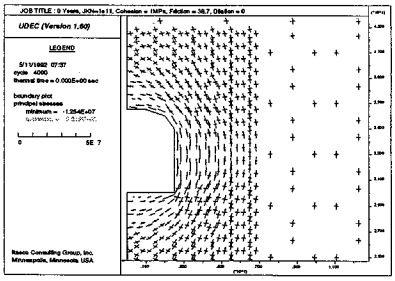

核廃棄物地中処理影響解析

■販売条件

UDEC・3DEC・FLAC

- ◆EWS（SUN-SPARC）
- ◆IBM-PC/AT及び互換機
- ◆UDECはソースコードで提供します。
- ◆3DEC・FLACはロードモジュールで提供します。

FLAC

有限差分法(FDM)プログラム

FLACは個別要素法コードUDEC，3DECを発表したDr.P.Cundallが同様の有限差分ロジックを用いて連続体の塑性大変形の解析するために開発したコードで、現在、全世界で数多く使用されています。有限差分法は、地盤、岩盤を有限な領域内で離散化し、連動方程式と構成則を差分方程式として解析するもので、有限要素法に比べ非線形大歪が扱えることで大きな優位性を持っています。
FLACは小ー大歪　非線形、動的ー静動挙動を始めとし、豊富な機能　オプションを備えたPC、ワークステーション用の地盤解析コードです。

オプション

- ■ダイナミック解析モデル
- ■クリープ解析モデル
- ■熱解析モデル

適用分野

- ●斜面・盛土の設計、安定解析
- ●浅／深基礎設計
- ●アースダム、コンクリートダムの設計
- ●トンネルの設計
- ●核廃棄物貯蔵解析
- ●液状化解析

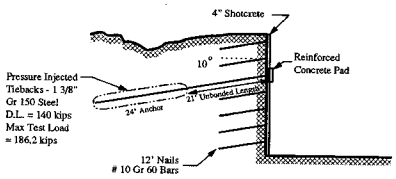

地盤安定解析

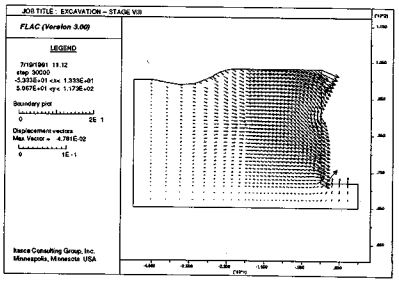

株式会社CRC総合研究所　西日本支社

〒541
大阪市中央区久太郎町4丁目1-3
(06)241-4121　営業担当:岩　崎

土木学会論文集

昭和三十七年五月二十八日　第三種郵便物認可
平成五年八月十五日・印刷
平成五年八月二十日・発行
土木学会論文集（毎月一回二十日・二十一日発行）

定価＝1000円（本体価格・九七一円）